TECHNICAL MEMORANDUM

706

All-sky assimilation: better snow-scattering radiative transfer and addition of SSMIS humidity sounding channels

Alan J. Geer

Research Department

October 2013

European Centre for Medium-Range Weather Forecasts
Europäisches Zentrum für mittelfristige Wettervorhersage
Centre européen pour les prévisions météorologiques à moyen terme

Series: ECMWF Technical Memoranda

A full list of ECMWF Publications can be found on our web site under:
http://www.ecmwf.int/publications/

Contact: library@ecmwf.int

European Centre for Medium-Range Weather Forecasts
Shinfield Park, Reading, RG2 9AX, England

Abstract

The all-sky assimilation of microwave radiances has benefitted from removing the largest remaining systematic error in the observation operator. Previously, the optical properties of snow hydrometeors were computed using Mie theory but now it is possible to use the Discrete Dipole Approximation, which gives more accurate results for complex 3D particles like snowflakes. These improvements in the observation operator allow the all-sky assimilation to be extended into deep-convective areas and to the 183 GHz water-vapour sounding channels on SSMIS (Special Sensor Microwave Imager Sounder). There are clear benefits to midlatitude wind and geopotential forecasts as well as to humidity throughout the troposphere. Improved dynamical forecasts presumably come about because the forecast model inside 4D-Var is forced into a better fit to the observations of water vapour, cloud and precipitation. Scores are particularly helped by the mid and upper-tropospheric 183 GHz water vapour channels, likely through the wind tracing effect. The beneficial impact on winds cannot be replicated using a clear-sky assimilation strategy. This encourages efforts to widen the application of the all-sky approach to other microwave instruments with water-vapour, cloud and precipitation tracing capability such as MHS (Microwave Humidity Sounder). Further, it should encourage attempts to extend all-sky assimilation to the water vapour channels on infrared instruments.

1 Introduction

Traditionally, microwave imager radiances have been assimilated in clear-sky conditions to help improve lower-tropospheric humidity (Andersson et al., 2007) but more recently they have been assimilated in all-sky conditions (Bauer et al., 2010; Geer et al., 2010b). This extends observation coverage and helps improve cloud and precipitation in the analyses and forecasts. Though the 4D-Var control variable does not contain cloud or precipitation, the presence of linearised moist physics in the minimisation (Tompkins and Janisková, 2004; Lopez and Moreau, 2005) means that model cloud and precipitation are modified in the analysis in order to fit what is observed in the all-sky radiances. A key aspect in all-sky assimilation is a model for observation error that represents small errors in clear-sky conditions and much larger ones in cloudy and precipitating situations (Geer and Bauer, 2011). Errors are larger in cloud and precipitation due to the poor representativeness of the model, i.e. the inaccurate shape and location of cloud and precipitation features in the forecasts, as well as the increased difficulty of radiative transfer.

A remaining problem in microwave all-sky assimilation has been large systematic radiative transfer errors in deep-convective situations. Poor modelling of the scattering properties of snow hydrometeors results in excessive scattering at frequencies from 30 GHz to 90 GHz and insufficient scattering at higher frequencies. This has hindered the use of all-sky assimilation wherever snow scattering is the dominant radiative effect, particularly in the use of temperature and moisture sounding channels (e.g. Geer et al., 2012) and over land surfaces (e.g. Baordo et al., 2012).

The scattering properties of snow hydrometeors were previously computed using Mie theory, with snow represented as a sphere containing a mix of ice and air. However, the limitations of the Mie approach are widely recognised (Petty and Huang, 2010; Kulie et al., 2010). The Discrete Dipole Approximation (DDA, Purcell and Pennypacker, 1973; Draine and Flatau, 1994) is available to compute the scattering properties of complex 3-D shapes and tabulated results are now widely available (e.g. Liu, 2008). Moving to a DDA representation of snow hydrometeors has essentially fixed the largest remaining problem in all-sky radiative transfer (Geer and Baordo, 2013).

The improved DDA radiative transfer will be introduced operationally with cycle 40r1[1] and it has allowed

[1]Note that these changes were initially merged into the code and tested for cycle 39r1, but since that cycle was never made operational, this memo will refer to 40r1 for simplicity.

a number of extensions to the all-sky assimilation. The package of changes is:

- In the observation operator, DDA sector snowflakes will be used to represent the optical properties of snow hydrometeors, replacing the inaccurate Mie sphere approach.
- High frequency channels (e.g. > 30 GHz) will now be assimilated in deep convective areas, taking advantage of the improvements in the radiative transfer model.
- Observation errors have been recomputed.
- The Special Sensor Microwave Imager/Sounder (SSMIS) 183 GHz water vapour sounding channels will be actively assimilated for the first time.

All of these changes have beneficial impacts on the assimilation system but it is worth highlighting the use of the 183 GHz water-vapour sounding channels of SSMIS. Up until now, the all-sky system has only been used operationally to assimilate window channels at frequencies up to 90 GHz which mainly have sensitivity to the lower troposphere. All-sky assimilation of microwave temperature sounding channels has been tried, but it duplicates cloud information found in the window channels and adds noise to the temperature fields, so it has not been adopted operationally (Geer et al., 2012). In contrast, this study shows that 183 GHz microwave humidity sounding channels are well suited for all-sky assimilation and they bring useful new information on midlatitude winds, likely through the 4D-Var tracing effect. In clear skies these channels are sensitive to upper and mid tropospheric humidity (e.g Buehler and John, 2005) and ECMWF has been using similar channels on AMSU-B (Advanced Microwave Sounding Unit B) and MHS (Microwave Humidity Sounder) for many years for clear-sky humidity sounding. However, the 183 GHz channels are also strongly affected by scattering from snow and ice hydrometeors in deep convective systems (e.g. Hong et al., 2005), so the all-sky assimilation of these channels has had to wait for improvements in scattering radiative transfer.

2 Method

2.1 All-sky assimilation

The direct assimilation of all-sky radiances was implemented operationally in 2009, as described by Bauer et al. (2010) and Geer et al. (2010b). However, some additional developments were necessary to get the best out of this new approach: first, to start superobbing observations onto a T255 Gaussian grid before assimilation (about 70 km horizontal resolution) and to use a symmetric model for observation error (Geer and Bauer, 2010, 2011).

All-sky assimilation is currently applied to two instruments: SSMIS (Kunkee et al., 2008) on Defense Meteorological Satellite Programme satellite F17 (DMSP-F17) and TMI (TRMM Microwave Imager, Kummerow et al., 1998) on the Tropical Rainfall Measuring Mission (TRMM). There are also SSMIS instruments on DMSP-F16 and DMSP-F18 but these are not used as they are in similar orbits to DMSP-F17 and they are more affected by instrument issues associated with solar heating and solar intrusion (e.g. Bell et al., 2008). Solar-dependent anomalies are also present in the TMI data (e.g. Gopalan et al., 2009) but they are removed in the ECMWF bias correction (Geer et al., 2010a). See Sec. 2.3 for a description of the channels assimilated.

2.2 Radiative transfer improvements

The radiative transfer model for all-sky microwave assimilation is known as RTTOV-SCATT. It is a fast model designed for assimilating microwave radiances in all-sky conditions (Bauer et al., 2006) and it is a component of the wider RTTOV package (Radiative Transfer model for Television Infrared Observation Satellite Operational Vertical sounder; Eyre, 1991; Saunders et al., 2012). RTTOV-SCATT uses the delta-Eddington approximation (Joseph et al., 1976) to solve the radiative transfer equation including scattering. The four hydrometeor categories provided by the forecast model to RTTOV-SCATT are cloud water, cloud ice, rain and snow. Their bulk optical properties (e.g. single scattering albedo, extinction, asymmetry parameter) are taken from look-up tables.

The 40r1 radiative transfer upgrade was principally a change in the look-up tables of bulk optical properties. Previously the optical properties of snow particles were computed using Mie theory, i.e. using a perfect sphere to represent what are in reality quite complex 3D structures. Now, the Liu (2008) database of DDA optical properties is used. This database gives the optical properties of a range of ice and snowflake shapes at varying sizes and frequencies; integrating this information over the assumed size distribution of snow particles gives the bulk optical properties for input to RTTOV-SCATT. Using the 'sector snowflake' from the Liu database and a Field et al. (2007) particle size distribution gives a great improvement in the fit between model simulations and microwave observations in deep-convective areas, compared to the physically unrealistic results from Mie theory. More detail on the radiative transfer upgrade can be found in the forthcoming report by Geer and Baordo (2013). Much of their effort was devoted to finding the best choice of particle shape and size distribution using objective criteria based on a range of statistics of fit between model and observations. For global data assimilation it is important to find a particle shape that works well across all microwave frequencies and in all areas of the globe. It is not enough to look only at the RMS of departures as these can be fooled by the 'double penalty' effect. This report gives only a quick overview of the results or Geer and Baordo. The 40r1 upgrade also includes some small changes that will be part of RTTOV version 11, including the use of precipitation mixing ratio rather than fluxes as the input units; those changes do not have a significant impact on the results.

Figure 1 shows mean first guess (FG) departures for the month of June 2012 based on passive monitoring experiments. The usual quality controls have been relaxed so that only land, sea-ice and high-latitude observations have been excluded from the sample. Using the Mie sphere to represent snow hydrometeors produces excessive scattering at lower frequencies, leading to systematic positive departures particularly in the ITCZ regions and the maritime continent (e.g. 22, 37 and 52.8 GHz; panels a, c, e). In contrast at high frequencies the Mie sphere produces insufficient scattering, leading to negative departures in similar regions (183 GHz channels, panels g, i, k). If these biases were assimilated they could negatively affect the quality of the analyses. In order to prevent this, convective situations have been removed by quality control up until now (Geer and Bauer, 2010). Using the DDA sector snowflake removes the areas of positive bias completely in the 22v and 52.8 GHz channel and partially in the 37v channel (panels b, d, f), meaning that the quality control (QC) of convective situations can be relaxed. Negative bias in the 183 ± 7 GHz and ±3 GHz channels is decreased, making it safer to assimilate these channels in the all-sky route. The only area where biases have got larger is in the extratropics in the 183 ± 7 GHz, but it is impossible to improve fits everywhere at every frequency, and as shown by Geer and Baordo (2013) the DDA sector snowflake is still the optimal choice of particle shape across all microwave channels. A number of other statistics can also illustrate the scope of the radiative transfer improvements. Deep convective situations comprise only a few percent of all observations, so it is helpful to look at statistics which are more sensitive to these areas.

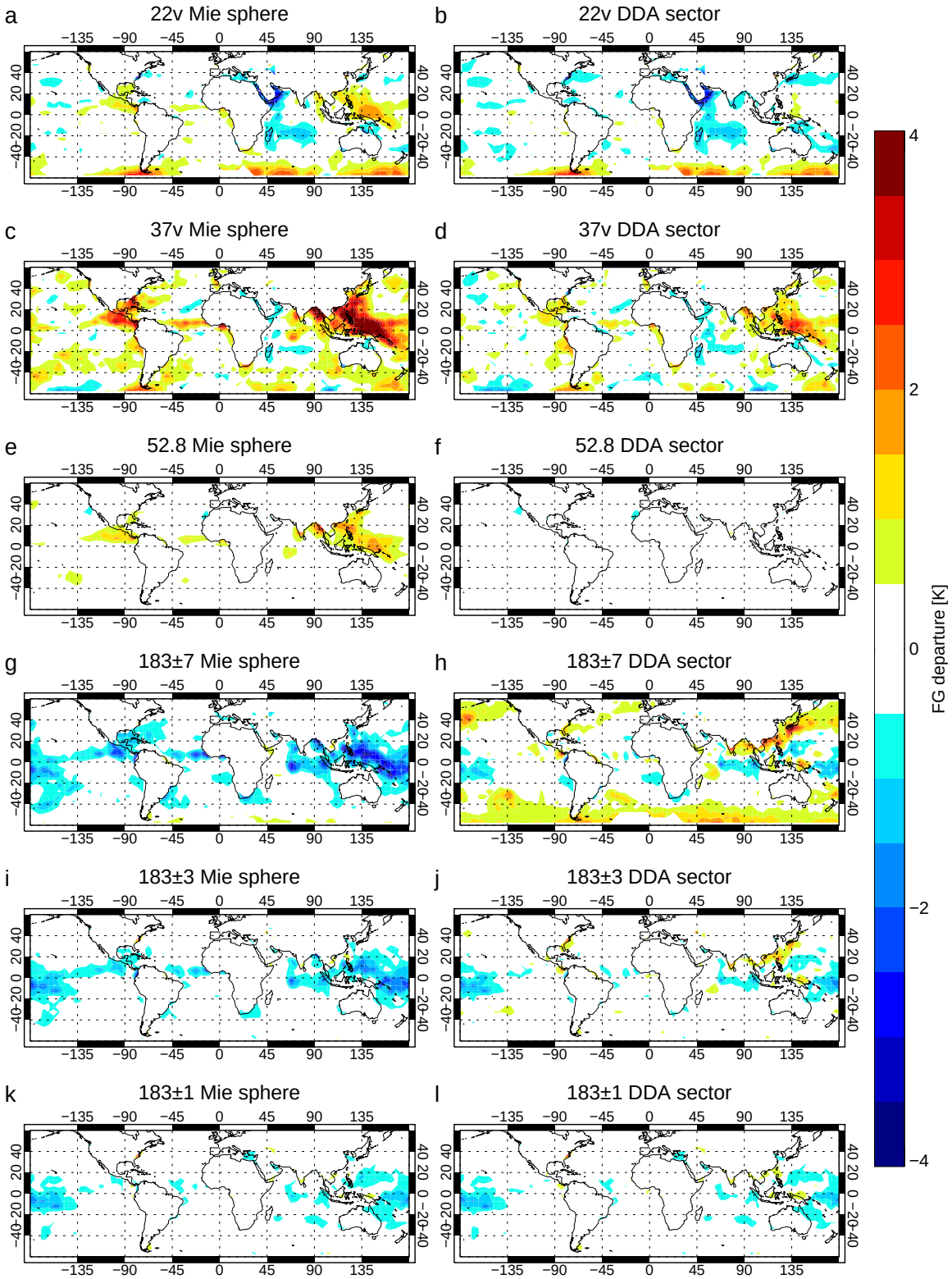

Figure 1: Mean first guess departure [K] for the month of June 2012, in all-sky conditions (i.e. clear, cloudy and precipitating) using Mie sphere (left column) or DDA sector snowflake (right column) to represent snow hydrometeor scattering, for a selection of SSMIS channels. A fixed VarBC bias correction has been applied; these results are based on passive monitoring experiments. Normal quality control has been relaxed, so that only land, sea-ice and high-latitude points are excluded.

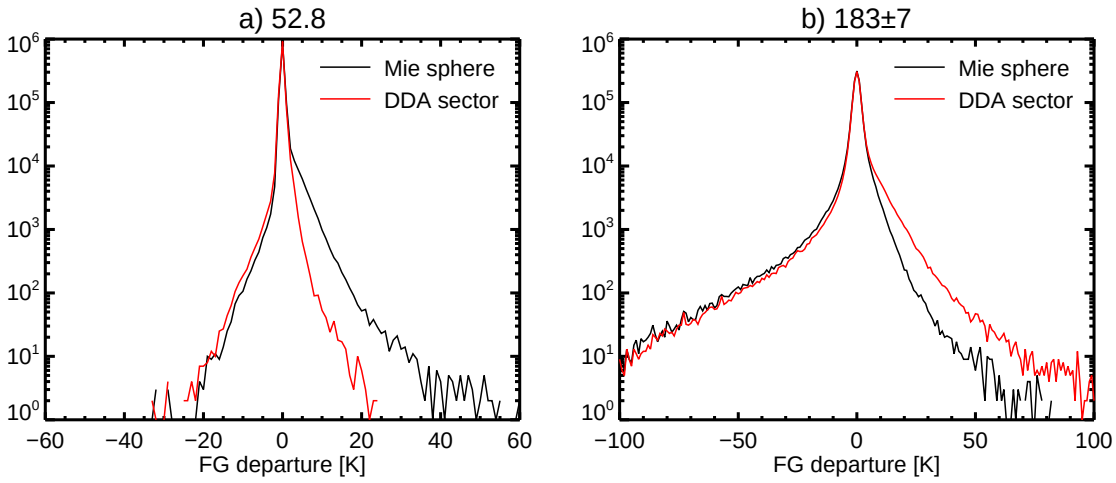

Figure 2: Histograms of FG departure [K] for the month of June 2012 for all-sky conditions, representing snow hydrometeor optical properties with either the Mie sphere or DDA sector snowflake, for the SSMIS channels at 52.8 GHz and 183±7 GHz. The y axis is logarithmic.

Figure 2 shows histograms of FG departures using a logarithmic y-axis to focus attention on the tails of the distribution. The tails are composed of the largest FG departures; these are caused by disagreement between the model and the observations in precipitation areas. If the disagreement between model and observations is due to random forecast errors, the histogram should be symmetric. An asymmetric histogram indicates the presence of biases in precipitating areas. At 52.8 GHz (panel a), the most strongly affected lower-frequency channel, the Mie sphere produces a tail of positive departures corresponding to situations where the FG brightness temperature (TB) is much too low due to unphysically excessive scattering. The DDA sector snowflake gives more realistic scattering and the shape of the warm tail becomes close to that of the cold tail. At 183±7 GHz (panel b) the Mie sphere gives a histogram that is lopsided in the other direction. There should be a warm tail corresponding to situations where the model has precipitation but the observations do not. However, the Mie sphere does not simulate enough scattering so it does not decrease simulated brightness temperatures enough to produce as many large positive departures as there are large negative departures in the cold tail. The DDA scattering model provides a more symmetrical distribution of departures, indicating the simulations are more physically realistic and give more scattering.

Finally Fig. 3a shows observations of the 37v channel on SSMIS in a section of the E Pacific containing the ITCZ around 5°N to 10°N, with the highest (red-coloured) brightness temperatures indicating areas of precipitation. There is also an area of frontal precipitation around 105°W, 25°S. Panel b shows the equivalent simulations from FG forecasts, using the Mie sphere approximation. In these simulations there are areas around 120°W, 6°N and 90°W, 12°N where brightness temperatures are depressed below 220 K because the Mie simulations give strong scattering from snow particles in deep convection. The observations never show such low brightness temperatures in deep convection, indeed deep convection is characterised by high brightness temperatures at 37 GHz. These come from relatively warm emission from water cloud and rain and even intense hurricanes show a warm signature, not a cold one (Geer and Baordo, 2013). Scattering is clearly not a dominant process in reality so the strong scattering from the Mie sphere simulations must be unrealistic. Panel c shows the actively assimilated observations: a QC has been applied that removes observations in areas with deep convection in the model or observations; note there are also a few areas around islands which have been removed as a precaution against land

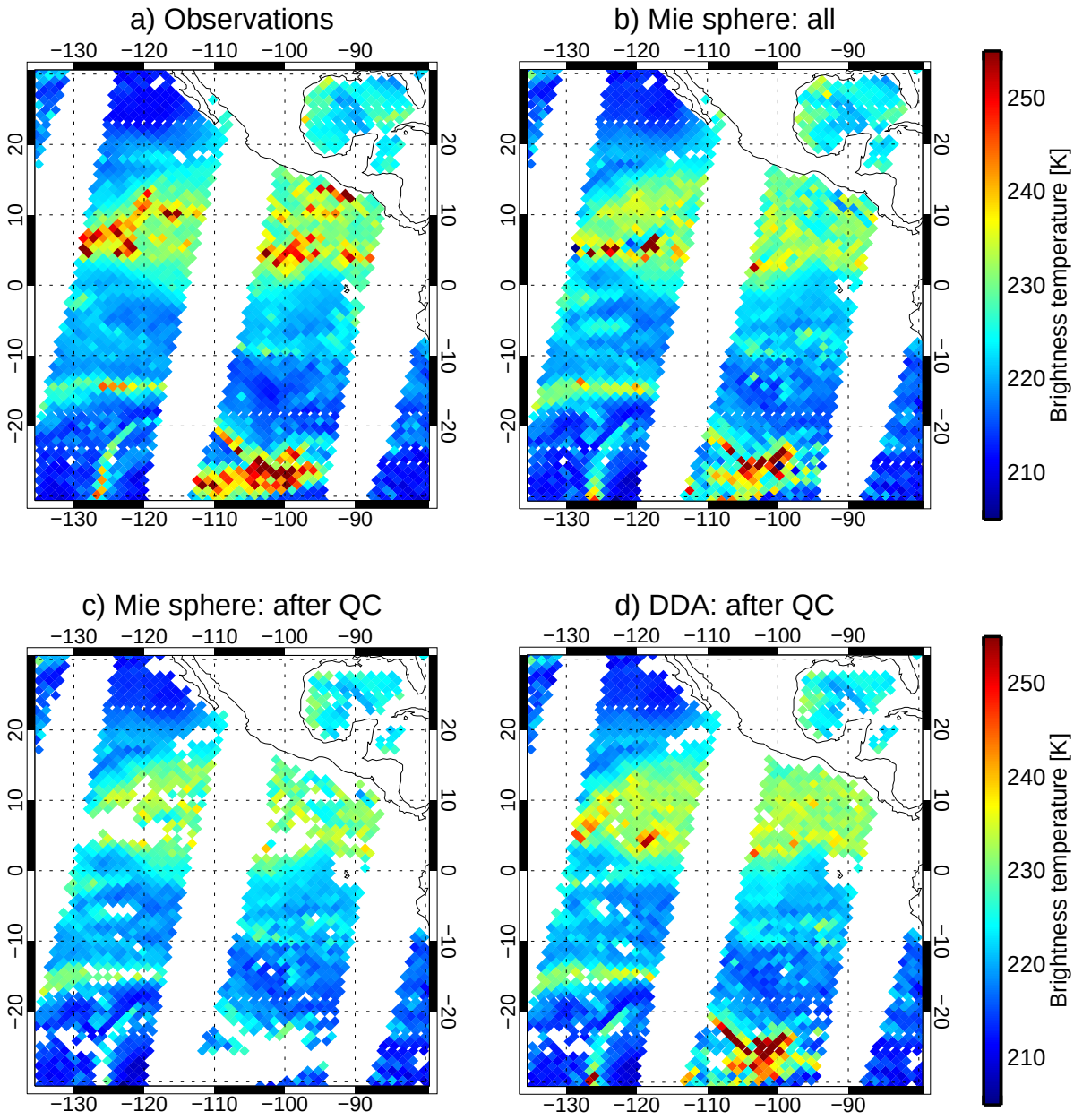

Figure 3: (a) DMSP-F17 SSMIS channel 37v observations on 2nd July 2013 and equivalent FG simulations with snow optical properties given by: (b,c) Mie spheres; (d) DDA sector snowflakes. Panels a and b show all available observations; panels c and d show the actively used data.

Table 1: Observation errors for the TMI and SSMIS channels to be assimilated at 40r1.

Name	Frequency [GHz]	Polarisation	Main atmospheric sensitivity over ocean	Clear-sky error [K]		Cloudy-sky error [K]	
				Old	New	Old	New
			TMI				
19v	19.35	v	Rain and cloud	2.8	1.7	15	19
19h	19.35	h	Rain and cloud	4.4	2.8	30	38
21v	21.3	v	Column water vapour	2.8	2.3	8	11
37v	37.0	v	Humidity, cloud	3.4	1.7	18	18
85v	85.5	v	Humidity, cloud, snow	3.9	1.7	18	16
			SSMIS				
19v	19.35	v	Rain and cloud	1.7	1.7	17	18
19h	19.35	h	Rain and cloud	3.9	3.9	32	32
22v	22.235	v	Column water vapour	2.3	2.3	8.9	8.4
37v	37.0	v	Humidity, cloud	1.7	1.5	14	18
91v	91.66	v	Humidity, cloud, snow	1.7	2.0	5.9	18
183±7	183±6.6	h	Lower trop. humidity	-	2.5	-	25
183±3	183±3	h	Mid trop. humidity	-	1.7	-	18
183±1	183±1	h	Upper trop. humidity	-	1.7	-	10

contamination. The QC for convective areas is a blunt instrument: it has removed the observations in the area of frontal rain to the S where the simulations look reasonable but it has left some areas of suspiciously low simulated brightness temperatures in the ITCZ (e.g. around 95°W, 9°N) where the model is giving unphysical scattering. With DDA sector snowflake radiative transfer the simulations are more realistic and the QC for deep convective areas can be switched off (panel d) giving a much better coverage of precipitating areas. There is still a qualitative difference between the model and observations in the ITCZ which could come from an underestimation of precipitation intensity and coverage in the model or alternatively might be a remaining radiative transfer issue. However, this is just a single example and the monthly means in Fig. 1 suggest that model and observations are unbiased in this area over longer periods.

To summarise, the use of the Mie sphere to represent snow particles was responsible for an unphysically high amount of scattering at lower frequencies (e.g. between 30 GHz and 90 GHz) that made it impossible to assimilate observations in precipitating areas in channels with these frequencies. The DDA representation for snow optical properties is more realistic and allows observations these observations to be assimilated for the first time. At 183 GHz the move to DDA again improves the realism of the simulations, by increasing the amount of scattering from snow particles, though the improvements are not so dramatic as in the lower frequencies.

2.3 Observation error retuning

New coefficients have been computed for the observation error model for TMI and SSMIS channels (Tab. 1) following the method of Geer and Bauer (2010, 2011). The observation error model is a linear function of the symmetric cloud amount, e.g. the average of observed and simulated cloud. Errors are at a minimum in completely clear-sky situations and a maximum in completely cloudy situations (in practice, this means strongly precipitating, deep convective areas). FG departures are binned according to the cloud amount. The standard deviation in these bins is known as the total error and the observation error is computed from this by removing a small amount representative of background error (1.0 K).

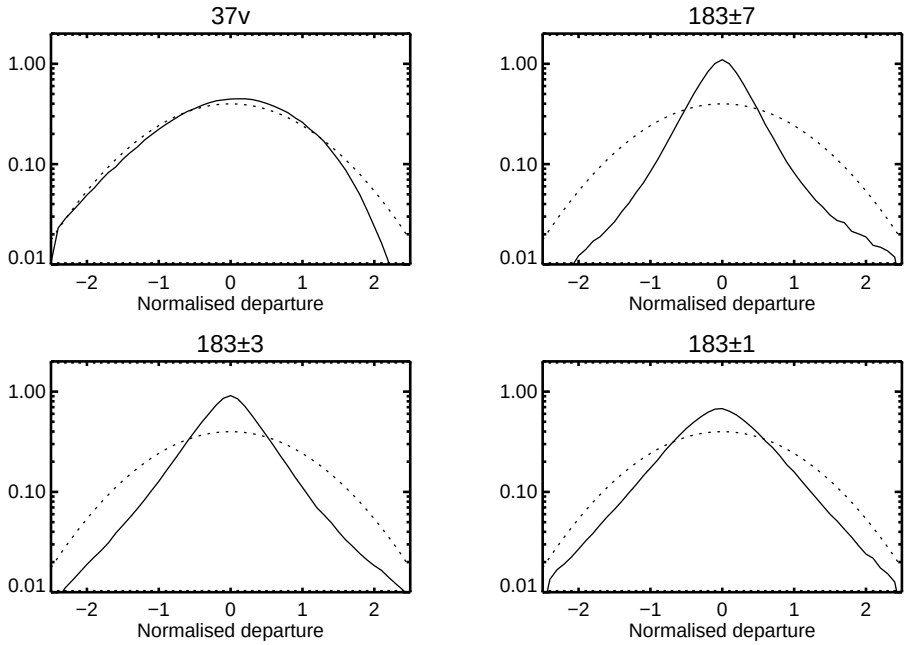

Figure 4: Log histograms of normalised FG departure (bias corrected departure divided by the applied observation error, solid line) for the month of July 2013 from an experiment using the new all-sky developments for 40r1. The dashed line shows a Gaussian with a standard deviation of 1.

The improved scattering has only a small effect on the quality of radiative transfer in lower-frequency channels (e.g. 19v, 19h, 21/22v) and the SSMIS errors in these channels remain essentially unchanged. The size of TMI clear-sky errors appears to have decreased at these frequencies, but this is unlikely to be related to the radiative transfer upgrade and probably just suggests that TMI errors were out of date. The TMI observation errors are now more similar to those of the equivalent channels on SSMIS, which is reassuring.

Deep convective areas are assimilated for the first time in the 37v and 85/91v channels and because these situations are associated with the largest FG departures, this requires a larger maximum error in cloudy skies than before. For example, the maximum error for SSMIS 91v goes from 5.9 K to 18.0 K. Finally, the 183 GHz channels have been assigned errors for the first time. In clear skies, these are comparable to the equivalent channels on MHS, which are all assigned a 2.0 K error.

Figure 4 shows the normalised departures in channels in channel 37v and the three channels at 183 GHz (normalised departure is the FG departure divided by the total error predicted by the symmetric error model). As expected the departure distribution is very close to Gaussian for channel 37v and for the other window channels (not shown). The symmetric error model does not work quite so well for the 183 GHz channels, particularly 183±7 GHz. However the modelled error distribution produces normalised departures that are predominantly quite small compared to the Gaussian, which means the errors are over-cautious. There is no danger in using this error formulation but in the future it might be possible to get more impact from the observations by targeting the error model more precisely. One aspect that would need reviewing is that in the 183 GHz channels, particularly the higher-peaking channels, forecast errors in clear-sky water vapour can sometimes produce nearly as large brightness temperature departures as those associated with poorly-forecast cloud or precipitation. There is scope to improve the error model for the 183 GHz channels, but as the results will show, it is fine to start with.

The effectiveness of the observation error model (along with the quality of the simulations, the effectiveness of quality control and bias correction) can also be tested by looking at normalised FG departure biases. With a highly variable observation error, it is better to check for systematic errors in the normalised departures than in the differences in absolute brightness temperature. Figure 5 shows that after bias-correction, remaining systematic errors in the 183 GHz channels are small compared to the observation error (panels f-h); in fact they are smaller than the systematic errors we tolerate in the window channels (panels a-e). The 183 GHz channels should be quite safe to assimilate. In all channels, biases are relatively small in normalised terms in the ITCZ and other convectively-active areas. Even though there are some remaining biases between model and observations in these areas (e.g. Fig. 1), the large size of the observation errors assigned in convective situations means the biases will not be dangerous for the data assimilation. Instead the largest biases in normalised departures are in the 37v and 91v channels in the maritime stratocumulus regions to the W of most continents in the subtropics, and also at high latitudes in the southern hemisphere (SH), where the long-standing 'cold-sector' bias is a problem (e.g. Geer et al., 2009; Geer and Bauer, 2010). The majority of situations affected by cold-sector bias are removed by QC, but there may be a residual of scenes escaping detection. Alternatively there might be an asymmetry in the quality control. However, none of these biases are larger than 0.7 in terms of normalised departure and the affected areas are small in extent. Overall, systematic error is small and unlikely to cause problems in the assimilation.

3 Results

3.1 Separate impact of the components

Initial testing of the all-sky developments was done at a horizontal resolution of T511 and vertical resolution of L91 for the 4 month period of June to September 2012. The all-sky developments were added in two stages, making it possible to separate the impact of the 183 GHz channels from the other developments. The experiments were:

- *Control*: A basic cycle 38r2 experiment
- *DDA scattering*: This uses the new scattering parameters and revised observation errors. Observation coverage is extended into deep convective areas in the 30 - 90 GHz channels where previously these observations were removed by quality control.
- *183 GHz channels on SSMIS*: As *DDA scattering* but also activating the 183 GHz channels on SSMIS. This is equivalent to the complete package that was supplied for 40r1.

Figure 6 shows the normalised change in RMS forecast scores in relative humidity, vector wind and geopotential at the levels where there is the greatest impact for each parameter. In all cases the verifying analysis is the 'own-analysis' of the experiment. There is a particularly beneficial impact of the complete package (e.g. the 183 GHz experiment vs the control) on relative humidity, winds and geopotential in the southern hemisphere and tropics. The impact is nearly 1% and is significant through most or all of the forecast range. Figure 7 shows the vector wind scores for this experiment resolved by latitude and pressure: beneficial impacts are seen at all latitudes and throughout the troposphere. Because the forecasts have been verified against their own analyses, the change in RMS errors at T+12 is equivalent to the change in the RMS increment in vector wind (e.g. Geer et al., 2010b). Hence, the package reduces the size of wind increments, indicating improved winds in the FG, and the impact persists in the forecasts for many days.

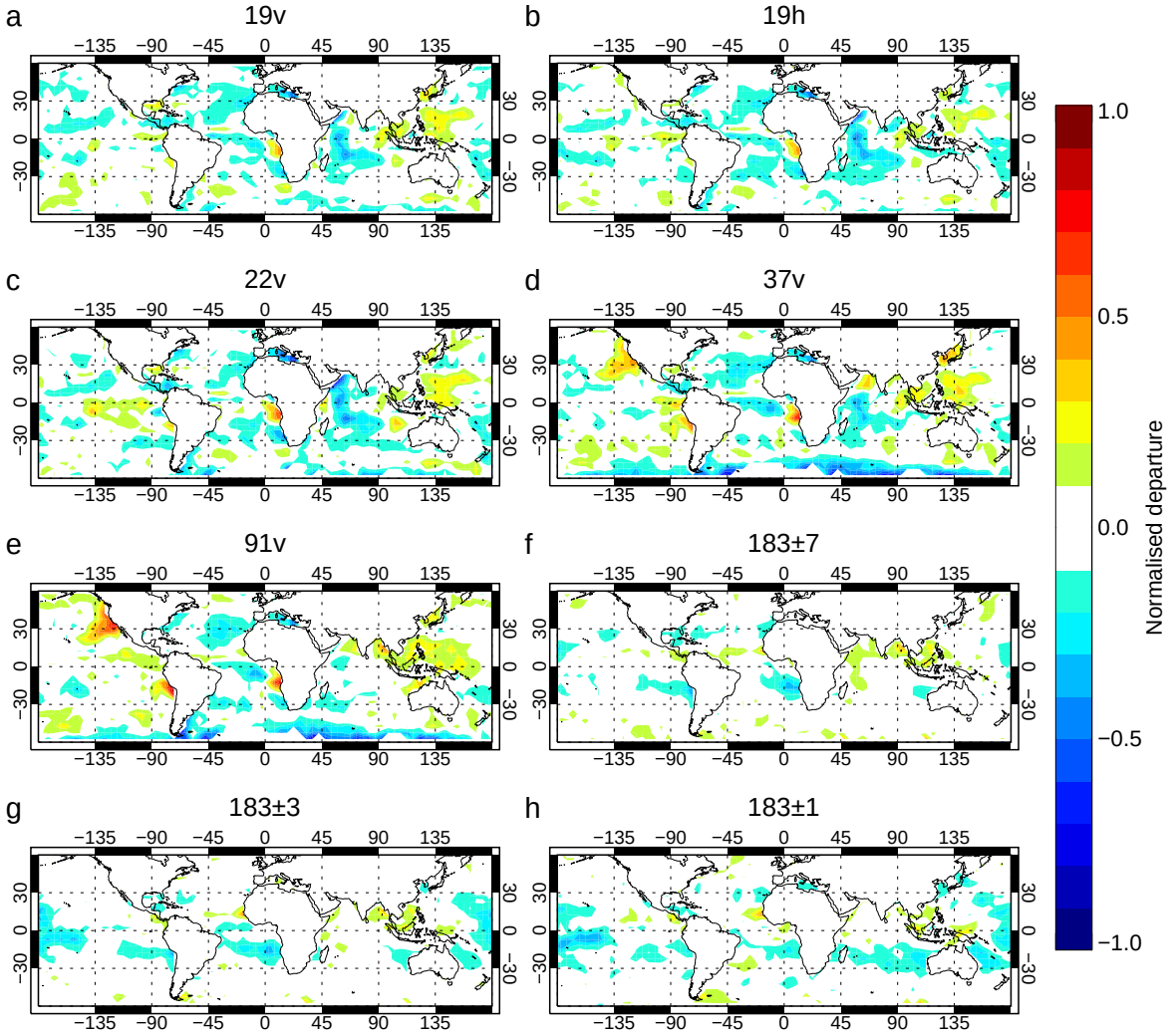

Figure 5: Maps of mean normalised FG departure (bias corrected departure divided by the applied observation error) for assimilated SSMIS observations for the month of July 2013, from an experiment in which the new configuration is used.

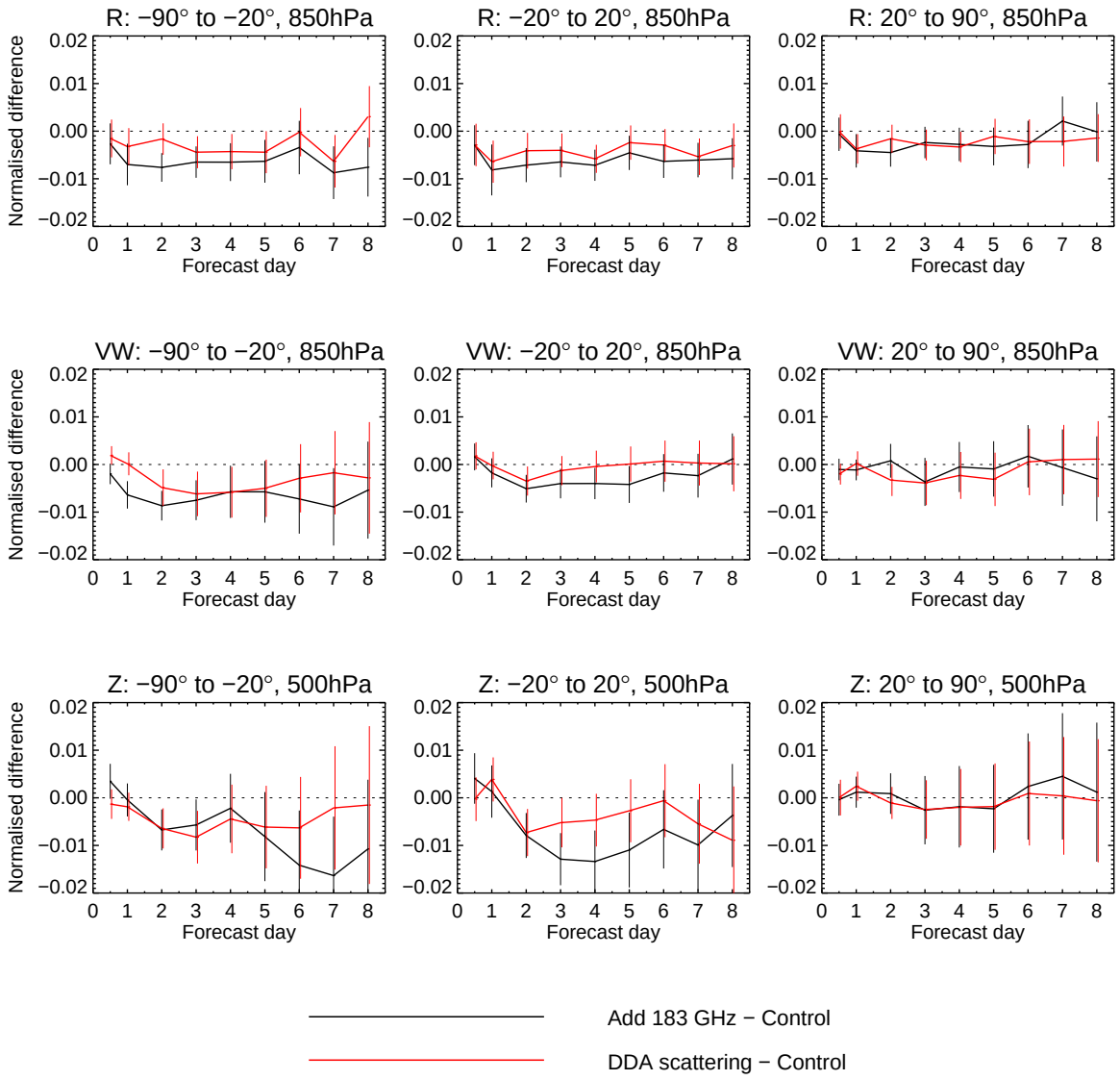

Figure 6: Normalised change in RMS forecast error in relative humidity at 850 hPa (top row), vector wind at 850 hPa (middle row) and geopotential height at 500 hPa (bottom row). Verification is against own analysis and scores are based on a four month period, June to September 2012. Error bars show the 95% confidence level. A beneficial impact is one that results in a reduction in forecast error, i.e. a negative normalised difference.

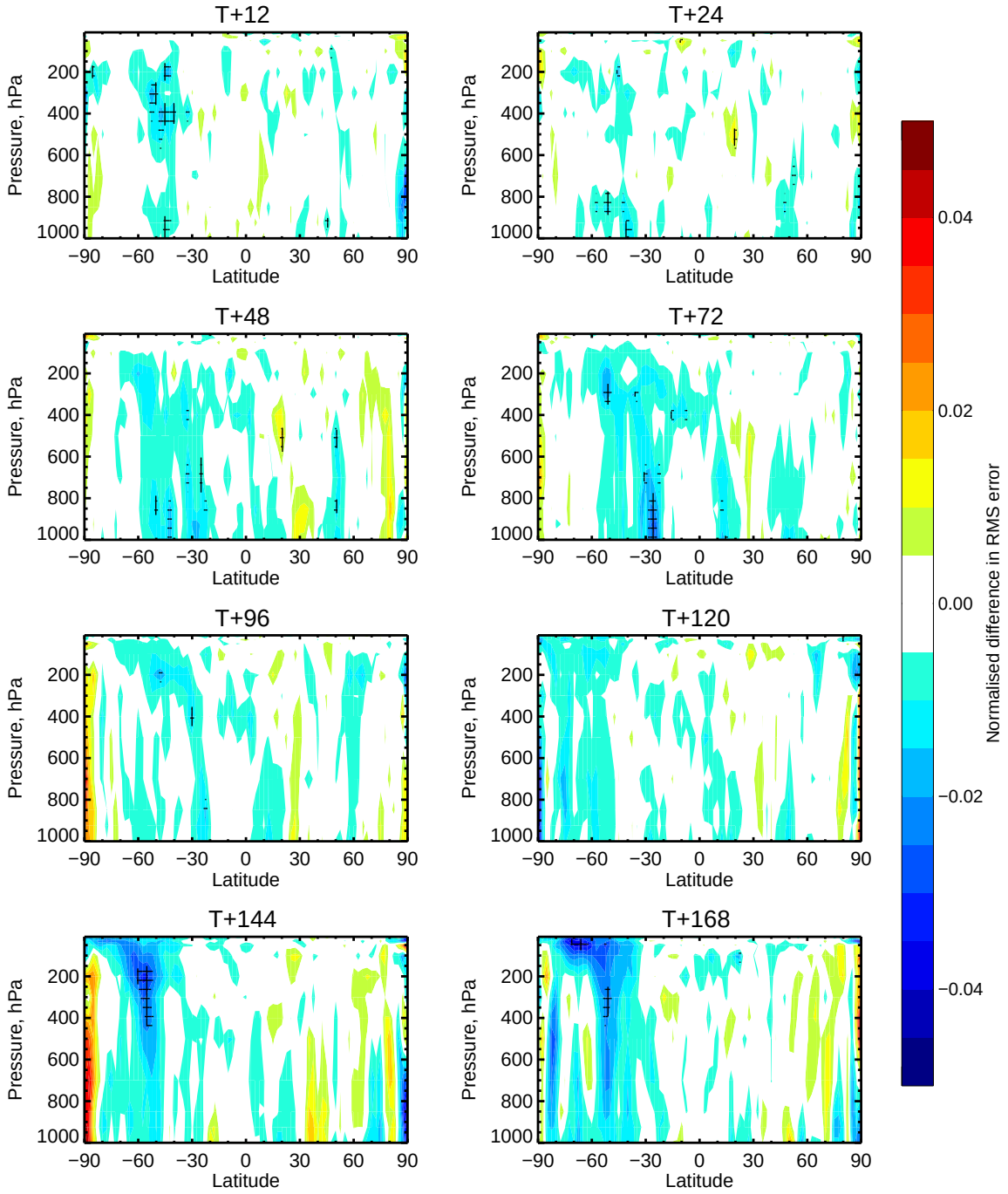

Figure 7: Normalised change in the RMS of vector wind forecast error between the 183 GHz channels experiment and the control (this tests the complete package of changes for 40r1). Verification is against own analysis and scores are based on a four month period, June to September 2012. Cross-hatched areas show changes that are significant at the 95% confidence level, after accounting for multiple comparisons. A beneficial impact is one that results in a reduction in forecast error, i.e. a negative normalised change. This is indicated by blue colours.

The wind impacts at longer ranges in the southern hemisphere (e.g. T+144 and T+168, Fig. 7) are significant in the stratosphere as well as in the upper troposphere. This is a period in which the stratosphere is dynamically active, due to the presence of the polar vortex, and the improved forecasts might be associated with an improved representation of polar stratospheric winds. Additional testing at a different resolution (T1279, not shown) extended this experiment into November 2012 when the polar vortex was breaking down. Similar patterns of improvement were seen in the scores. The all-sky observations improve upper-tropospheric winds in the SH storm tracks in the analysis, and these improvements may be propagated into the polar stratosphere during the forecast.

Figure 6 shows that both parts of the all-sky package contribute to the forecast scores, but in the SH it is the 183 GHz water vapour sounding channels that provide much of the initial improvement in winds, as well as the improvement in wind and geopotential beyond day 5.

3.2 Clear-sky versus all-sky assimilation for the 183 GHz channels

It is noteworthy that the 183 GHz water vapour sounding channels of SSMIS are beneficial to forecast scores, because MHS, with three similar water vapour sounding channels, shows little impact on dynamical scores when assimilated in the clear-sky path (not shown, but based on a one-year experiment denying MHS on Metop-A from the full observing system at cycle 38r2). This might indicate that all-sky assimilation is superior to clear-sky assimilation or it might just be that the clear-sky assimilation needs to be improved, for example through increased coverage, retuned observation errors or better cloud-screening. If it were possible to get forecast benefits from the SSMIS 183 GHz channels using clear-sky rather than all-sky techniques, the clear-sky approach might be preferable because it would save computer time (scattering radiative transfer is relatively expensive), reduce complexity and avoid the 'double-penalty' problem of including cloud in the FG (e.g. Geer et al., 2012).

To test these ideas, an experiment was created with clear-sky assimilation of the SSMIS 183 GHz channels; this was done by turning off cloud and precipitation radiative transfer for these channels in the all-sky observation operator. Quality control was imposed following the approach used for clear-sky assimilation of MHS. Cloud-affected observations were identified by looking at the clear-sky FG departures in the 150 GHz channel. If these were greater than 5 K, the observation was screened out. Also, a 2 K flat observation error was imposed, just as for MHS. This additional experiment provides a clean way of comparing all-sky and clear-sky techniques.

The impact of SSMIS 183 GHz channels using all-sky and clear-sky approaches is shown in Figs. 8 and 9, which focus on the first 2 days of wind forecasts (the control for these comparisons is the 'DDA scattering' experiment.) Unlike the all-sky approach, the clear-sky approach has no impact on wind scores or (not shown) geopotential scores. The clear-sky assimilation of 183 GHz improves the FG wind fits to other observations (Fig. 10, RH panels) but the all-sky assimilation improves the fits more: Clear-sky assimilation makes statistically significant improvements to the conventional observation FG wind fits on two pressure levels (300 and 400 hPa). All-sky assimilation gives significant benefits at 250, 850 and 1000 hPa in the satellite wind fits and at 200, 500, 700 and 1000 hPa in the conventional wind fits. There is little impact on analysis fits in either experiment (LH panels), and anyway changes in observation fits to analysis are hard to interpret as the wind analysis may be locally dominated by the observations that are supposed to be the reference. The change in fit to the upper tropospheric moisture channels of MHS is only slightly more beneficial in the all-sky experiment than the clear-sky experiment (Fig. 11). But overall, the all-sky assimilation of 183 GHz channels is more effective at improving wind forecast scores and fits to wind observations than the clear-sky assimilation.

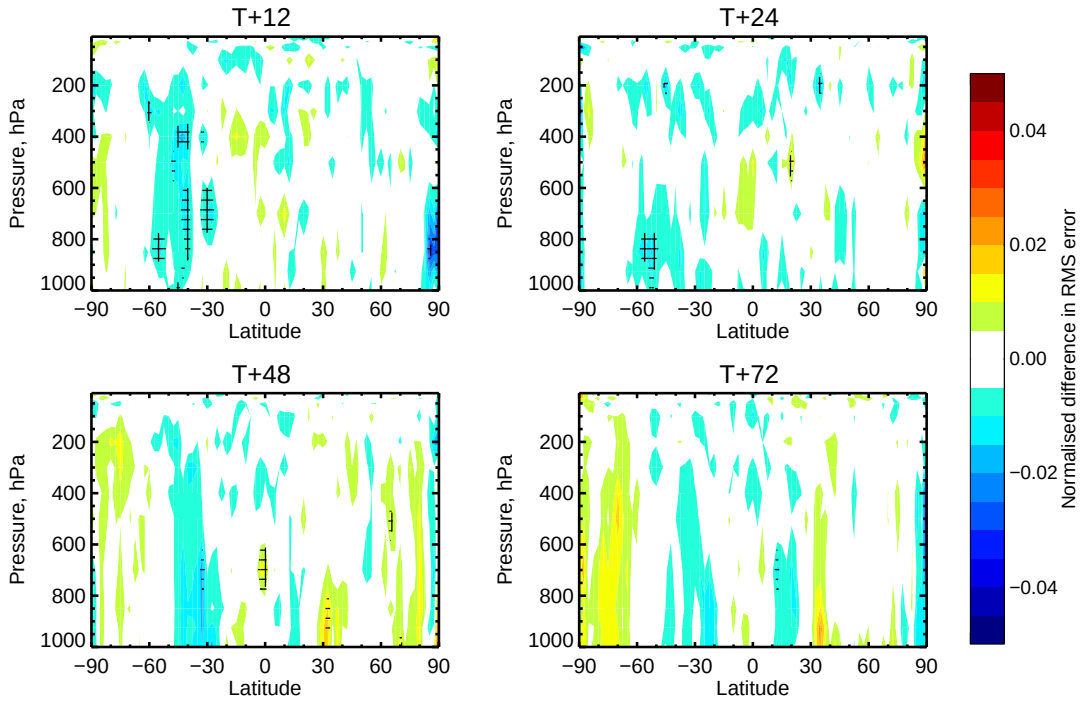

Figure 8: Effect of assimilating the SSMIS 183 GHz channels using the all-sky approach: normalised change in RMS forecast error in vector wind, based on experimentation for the period June-September 2012. Other details as Fig. 15

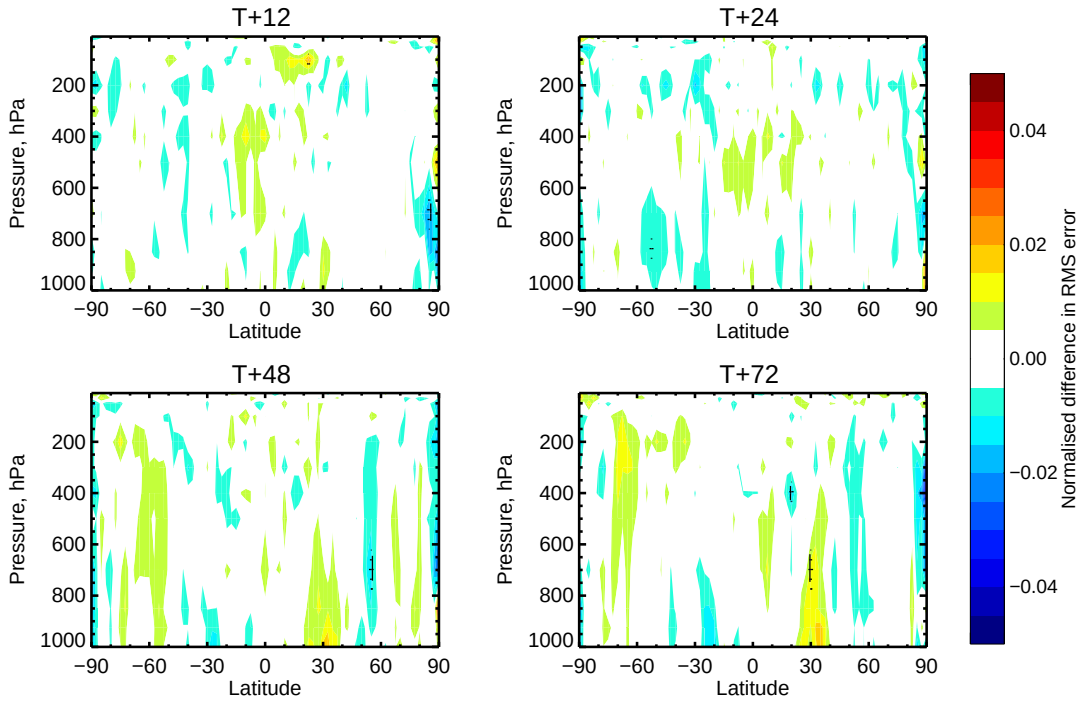

Figure 9: Effect of assimilating the SSMIS 183 GHz channels using the clear-sky approach: normalised change in RMS forecast error in vector wind. Details as Fig. 8

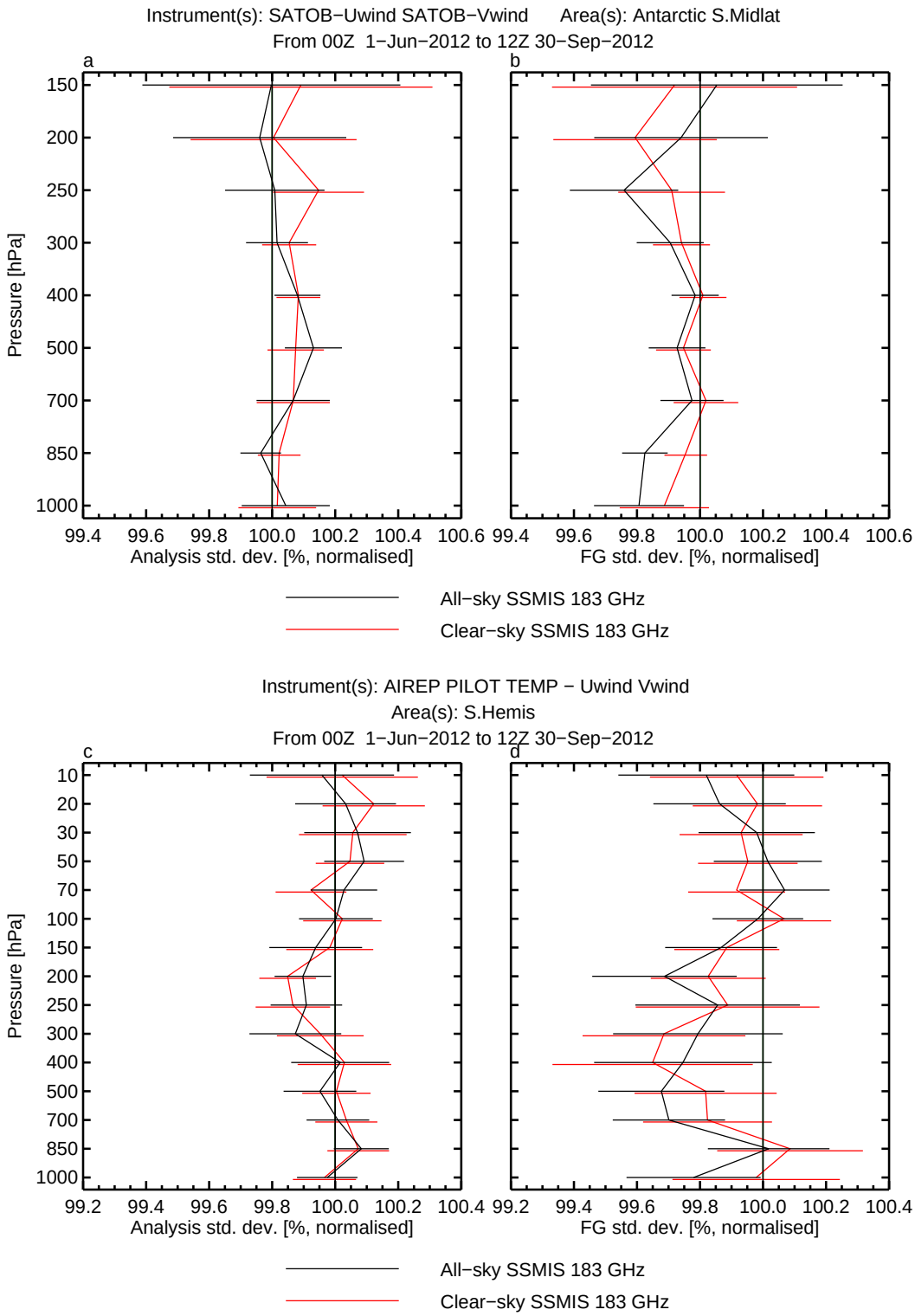

Figure 10: Normalised change in standard deviation of analysis (left) and FG (right) forecast departures for wind observations in the southern hemisphere, combining statistics from u and v wind components. Top row shows atmospheric motion vectors (AMVs) from satellites and bottom row shows conventional observations. Standard deviations are normalised by those of the control experiment. Error bars give the 95% confidence limits.

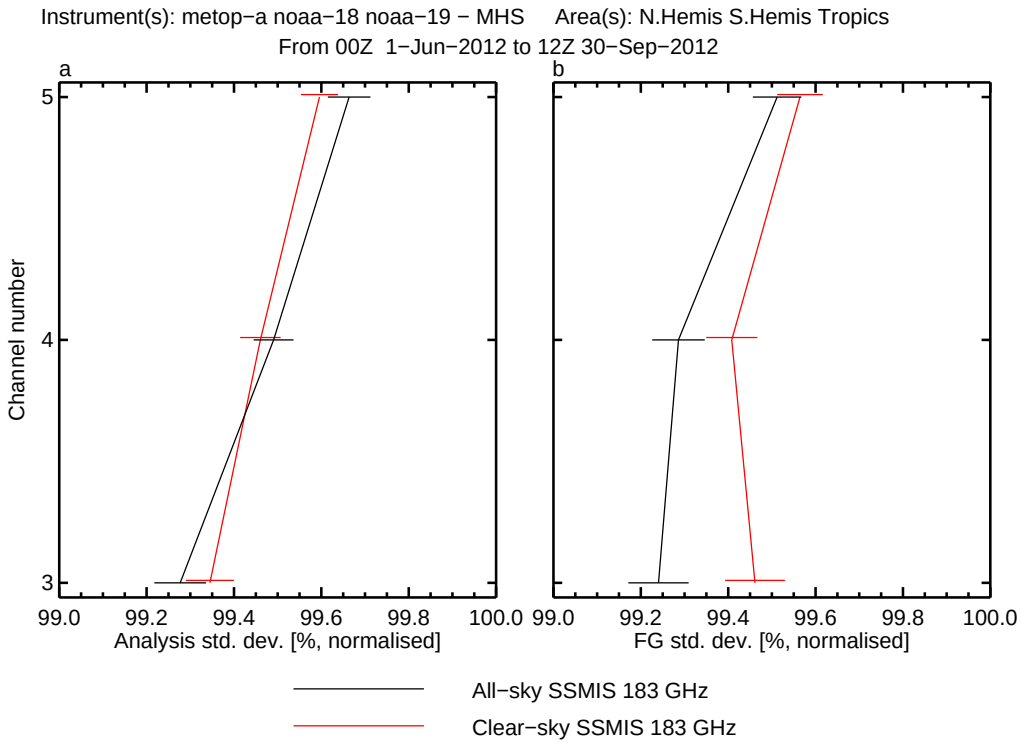

Figure 11: As Fig. 10 but for global MHS observations from NOAA-18, NOAA-19 and Metop-A.

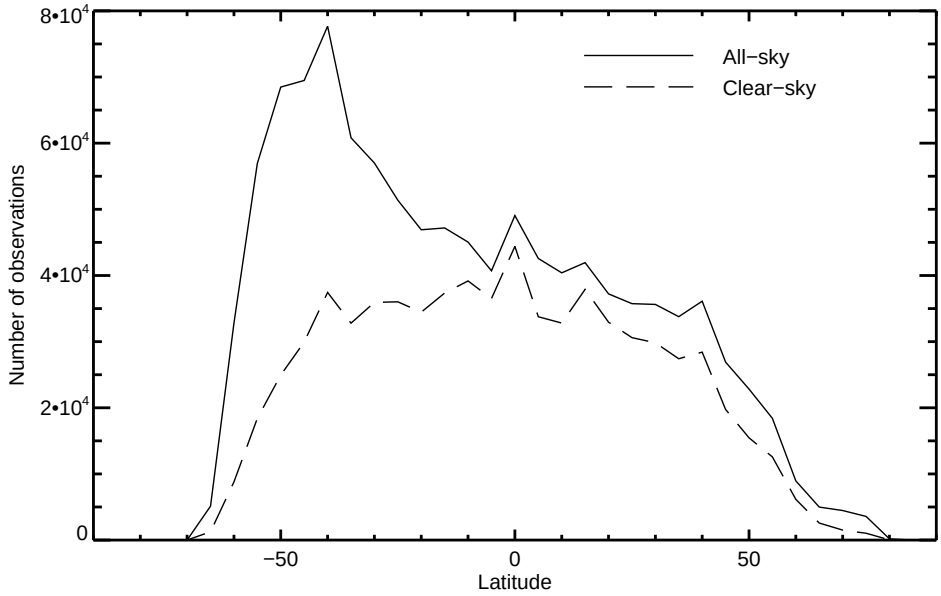

Figure 12: Number of observations in 5° latitude bins in July 2012 using either clear-sky or all-sky quality control.

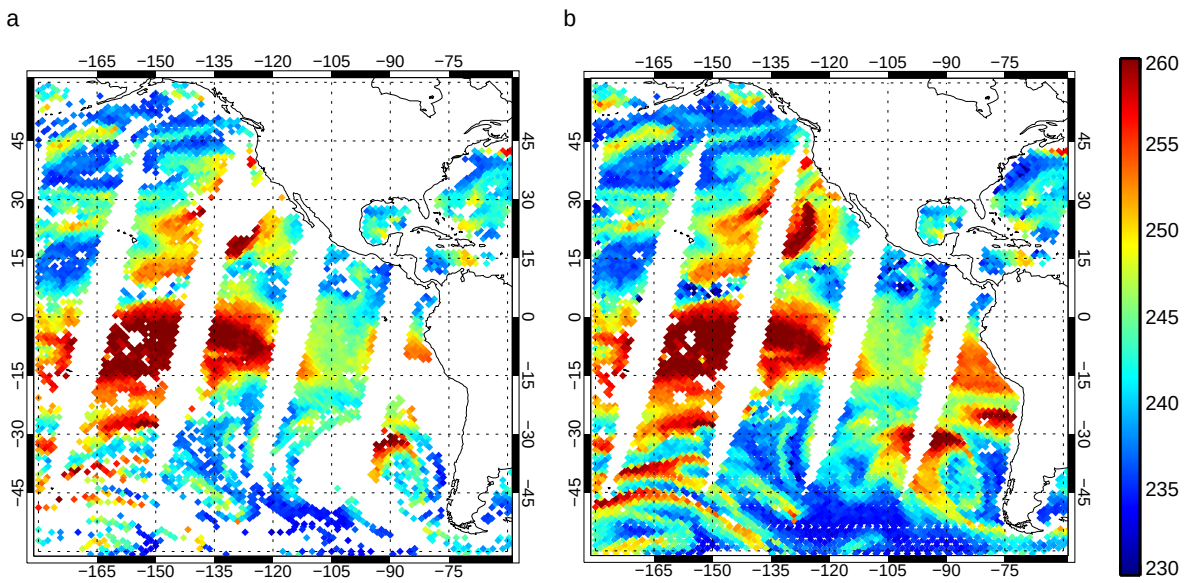

Figure 13: Observed brightness temperatures [K] from channel 183±1 of SSMIS in the 12Z analysis on 31st July 2012 after (a) simulated clear-sky quality control or (b) all-sky quality control.

To further understand the difference in forecast impact between the clear-sky and all-sky approaches, the coverage as a function of latitude is shown in Fig. 12 for the month of July 2013. All-sky brings two to three times more observations in the SH midlatitudes than does clear-sky. Coverage is lower in the NH because the all-sky approach is not yet applied over land surfaces, and the discrepancy between clear-sky and all-sky coverage is smaller, probably because in the summer season there is less cloud and precipitation. Fig. 13 shows maps of the 183±1 GHz observations assimilated in one cycle. There are large gaps in coverage in the clear-sky approach in the SH; cloud-screening removes a lot of observations.

Another issue with the clear-sky technique is the effectiveness of cloud-detection. This can be tested using simulated clear-sky and all-sky radiances. The 5 K cloud detection threshold can be applied to the all-sky minus clear-sky differences in the 150 GHz channel. The corresponding all-sky minus clear-sky differences in the 183 GHz channels indicate the effect on brightness temperature of the undetected cloud or precipitation. Table 2 gives the percentage of simulations that are affected by undetected cloud errors larger than 0.5 K or 2.0 K. The latter is relatively significant compared to the usual clear-sky observation error, also 2.0 K. The 183±7 channel is particularly susceptible to cloud-detection errors, with 8% of scenes affected by cloud errors of at least 2 K. The cloud-detection thresholds applied to MHS in the clear-sky technique could be tightened in the 183±7 channel. There may be some scope for loosening the threshold in the 183±1 channel. However, the all-sky approach brings much greater coverage and it may be that properly accounting for cloud and precipitation in the observation operator brings the additional benefits of cloud and precipitation tracing in 4D-Var.

Water-vapour sounding channels have long been known to provide an impact on wind fields through the 4D-Var tracer effect in clear-skies (e.g. Andersson et al., 1994; Peubey and McNally, 2009). The effect relies on the presence of gradients in fields such as water vapour or ozone and is most effective in regions where these gradients are strong and frequent, predominantly in the winter storm track regions (e.g. Riishøjgaard, 1996; Peuch et al., 2000; Allen et al., 2013). All-sky assimilation of microwave imager

Table 2: Percentage of simulated observations passing clear-sky quality control but still suffering from cloud biases, July 2013.

Channel	Percentage of scenes with undetected cloud error larger than:	
	0.5 K	2.0 K
183±7	21	8.2
183±3	11	2.1
183±1	2.0	0.0

channels in cloudy midlatitude frontal situations helped improve synoptic analyses in single-observation tests (Bauer et al., 2010), showing that cloud and precipitation tracing is perfectly feasible in the all-sky technique, and further, that 4D-Var is capable of inferring information from just a single observation. Sequential observations, though desirable (e.g. Allen et al., 2013) are not absolutely necessary.

In the present experiments, however, it is not completely clear how the improvements in wind forecasts come about. Clear-sky assimilation of 183 GHz channels is affected by errors associated with undetected cloud and the current cloud-screening provides less than half as many observations in the SH storm tracks than does all-sky assimilation. The all-sky may bring benefits simply because the additional observations improve the ability of 4D-Var to trace humidity features in cloud-affected areas. However, it is also likely that 4D-Var is directly tracing the cloud and precipitation features. It would be difficult to devise an experiment to investigate this further. Probably, all aspects are important, and anyway the microwave observations are progressively sensitive to water vapour, cloud and precipitation, with frontal features indicated in the observed brightness temperatures by elevated amounts of any or all of these (e.g. Fig. 13). Nevertheless, it seems reasonable to infer that the impact of the all-sky 183 GHz sounding channels on the wind fields comes through some combination of tracing of water-vapour gradients, cloud and precipitation and frontal features. The strong gradients in the storm-track regions, particularly in the winter, are the kind of features that could be tracked using the 4D-Var tracing effect; perhaps this explains the pattern of improvements in the SH in the austral winter experiments (Figs. 7 and 8). The experiments in the next section show similar impacts in wind forecast scores in the NH winter (no figure shown).

3.3 Impact of the complete package against the official 38r2 controls

Additional experiments were run against the official 38r2 control experiments at T511 horizontal resolution and 137 vertical levels. These experiments were required to justify implementation of the all-sky upgrade in cycle 40r1. Experimentation covers two three-month periods in 2012: January to March and June to August. The latter period overlaps with the T511/L91 testing described in the previous sections and over that same period, the results are very similar. The official testing gives the benefit of a longer period of experimentation (6 months) and winter and summer test cases.

Figures 14, 15 and 16 show the normalised change in RMS forecast errors for a selection of parameters, merging together the results from the summer and winter experiments to give 6 months total sample. The overall impression is that RMS errors decrease at shorter and longer ranges; there are no areas where the RMS errors increase. In many areas these changes are statistically significant, meaning that the all-sky upgrade makes a real improvement to the quality of forecasts at both shorter and longer ranges. RMS errors in vector wind are reduced by around 0.5% with statistical significance out to day 3 (Fig. 14). Though the most significant global impact is at 850hPa, there are also reductions in wind errors in the extratropical storm-track regions in the mid and upper troposphere (Fig. 15).

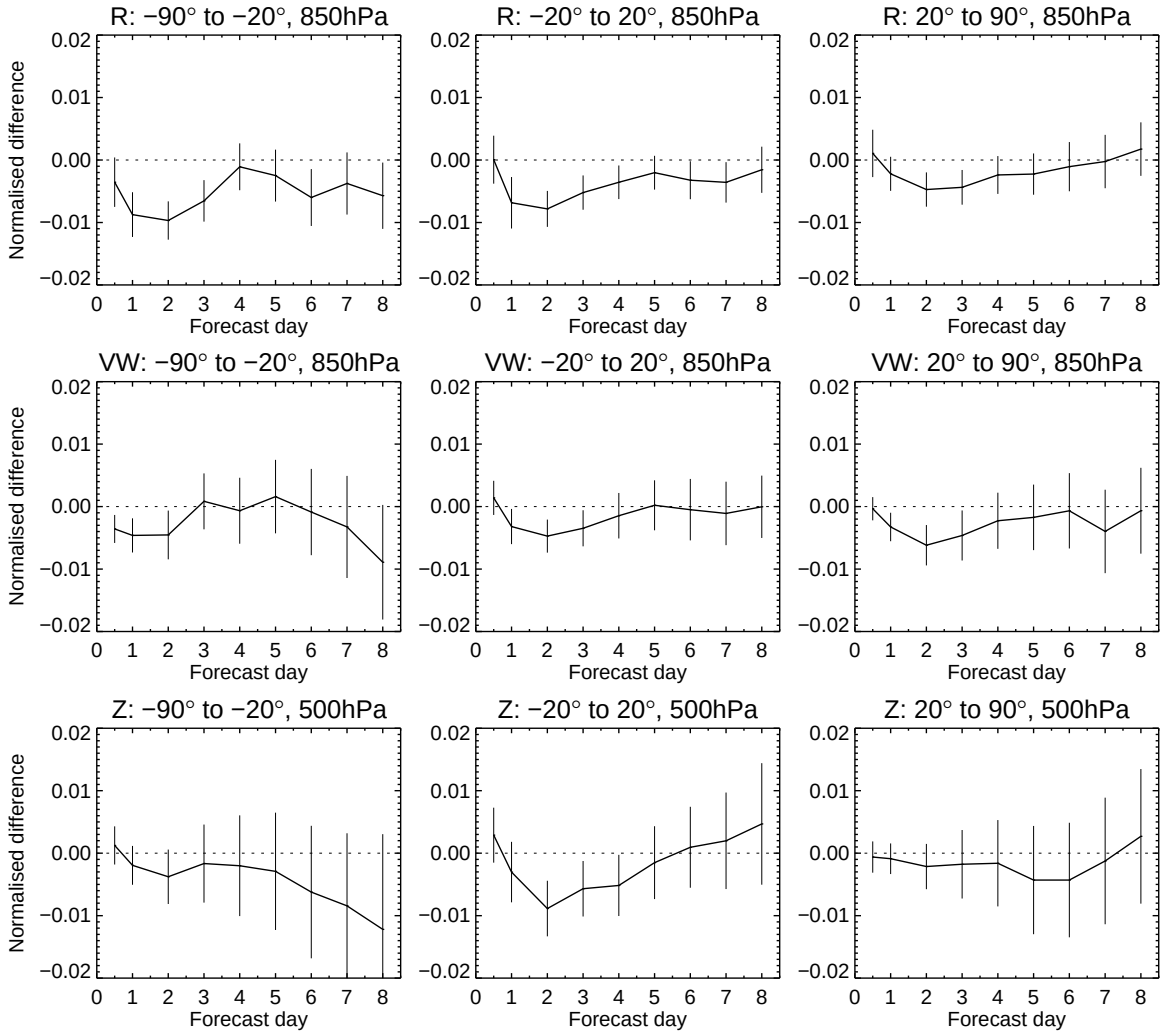

Figure 14: Normalised change in RMS forecast error in relative humidity at 850 hPa (top row), vector wind at 850 hPa (middle row) and geopotential height at 500 hPa (bottom row). These are the levels that show maximum impact for the different parameters. Verification is against own analysis and scores are based on the combined summer and winter experimentation totalling 6 months. Error bars show the 95% confidence level.

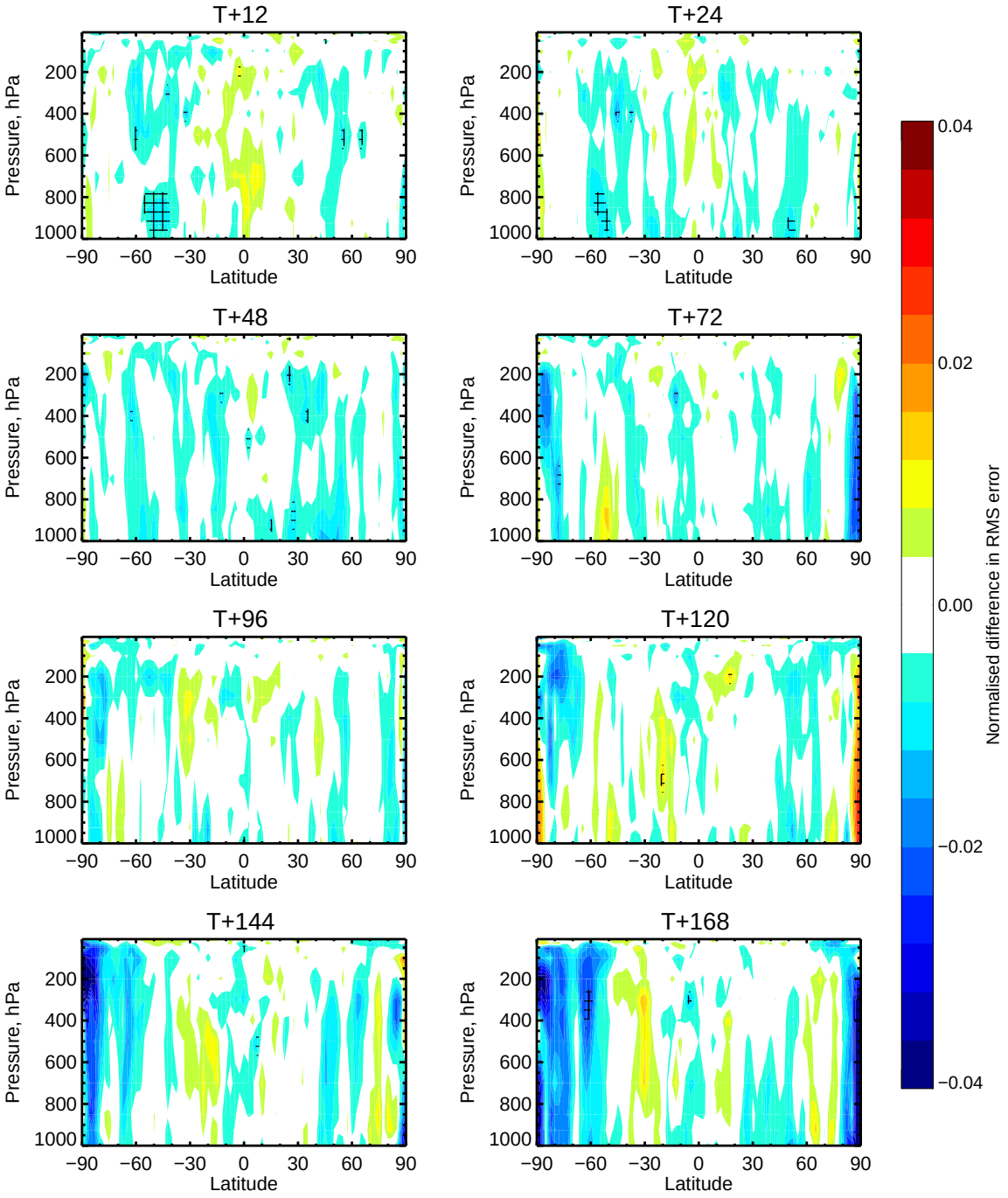

Figure 15: Normalised change in the RMS of vector wind forecast error. Verification is against own analysis and scores are based on the combined summer and winter experimentation totalling 6 months. Cross-hatched areas show changes that are significant at the 95% confidence level, after accounting for multiple comparisons.

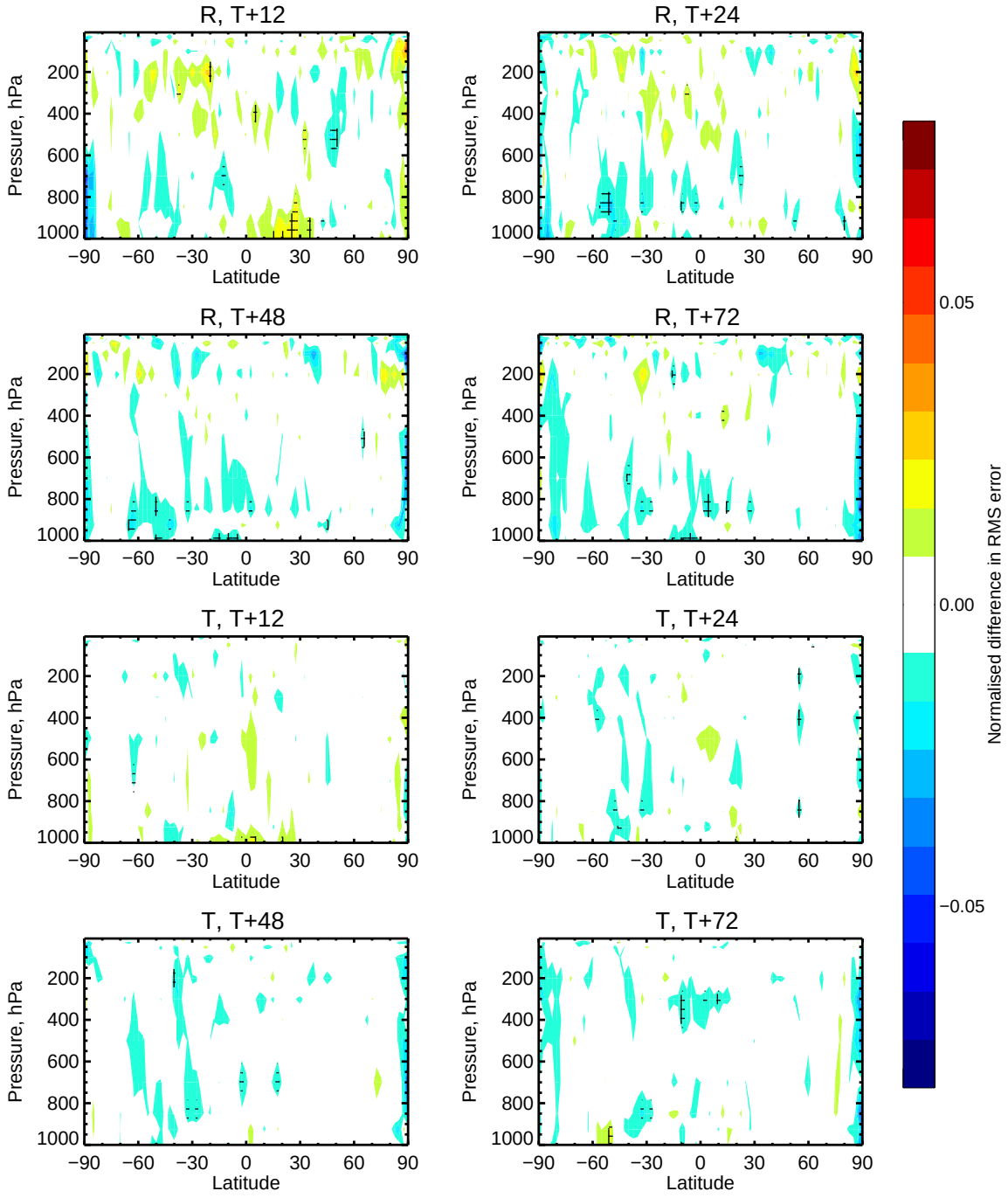

Figure 16: Normalised change in RMS of forecast error in relative humidity (R) and temperature (T) over the initial three days of the forecast (there is very little to see at longer forecast ranges). Verification is against own analysis and scores are based on the combined summer and winter experimentation totalling 6 months. Cross-hatched areas show changes that are significant at the 95% confidence level, after accounting for multiple comparisons.

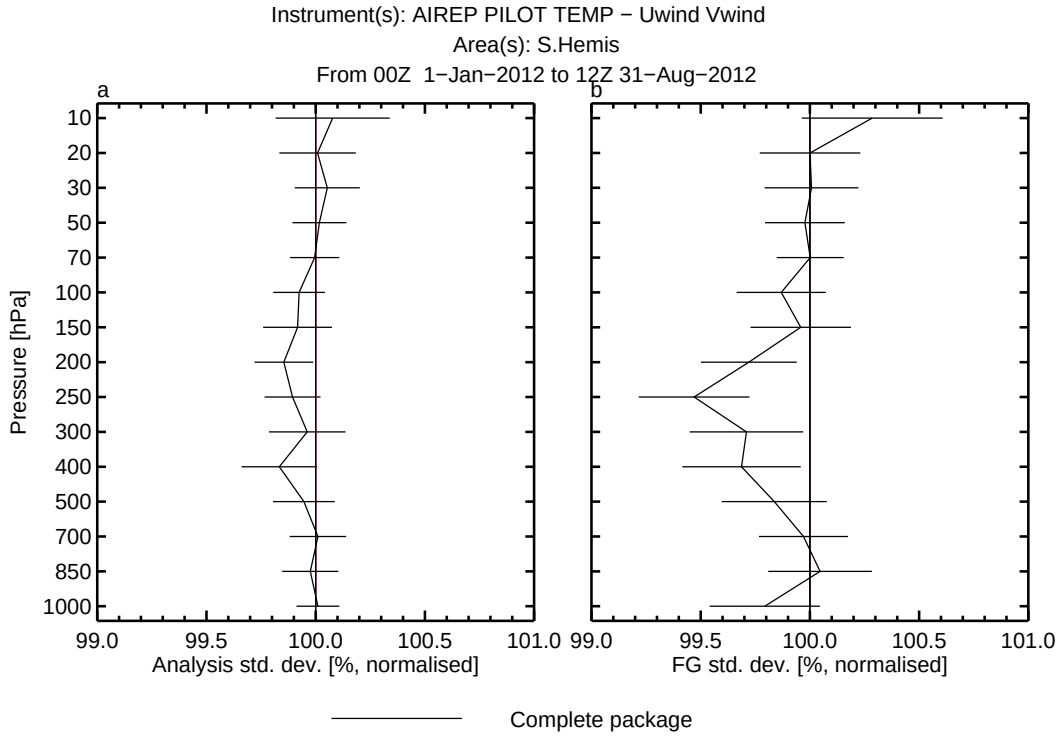

Figure 17: Normalised standard deviation of analysis departures (left) and FG forecast departures (right) for conventional wind observations in the southern hemisphere, combining u-component and v-component fits. Standard deviations are normalised by those of the 38r2 control experiment. Error bars indicate the 95% confidence interval.

Figures 14 and 15 show reductions in forecast errors in wind and geopotential in the southern hemisphere (SH) at longer forecast ranges (e.g. days 6 and 7), though these are not statistically significant over the combined 6-month period. This is interesting because these features are statistically significant in the austral winter experiment alone, e.g. June to August 2012, as in the T511/L91 experiments shown in previous sections. This might support the earlier suggestion that longer-range predictability came through the stratospheric polar vortex. In the austral summer, the stratosphere is dynamically quiet.

The fits to observations also show improvements. Figure 17 shows the normalised standard deviation of departures for conventional observations of wind in the SH in the combined winter and summer periods. The all-sky package reduces the standard deviation of FG and analysis departures by up to 0.5%; in the FG there is statistical significance in the upper-troposphere, on levels between 200 hPa and 400 hPa. Hence, the reductions in RMS wind forecast errors at T+12 in the SH storm tracks in Fig. 14 represent a real improvement in the quality of forecast winds.

We should not forget that winds are expected to be roughly in geostrophic balance with temperatures at the higher latitudes; thus temperatures would also be expected to be improved; this is confirmed by improved FG fits to radio-occultation (GPSRO) observations in Fig. 18. Here, there is significant improvement in the upper troposphere and lower stratosphere (vertical levels between roughly 9 km and 16 km) of about 0.3%. In the analysis, however, it is interesting that fits to wind instruments (Fig. 17a) are improved but the GPSRO fits are not. As mentioned before, we need to be very careful when interpreting changes in the analysis fit. But if we can believe it, it is evidence in support of the hypothesis that the wind-tracing effect is the mechanism by which the all-sky observations improve the dynamical forecasts.

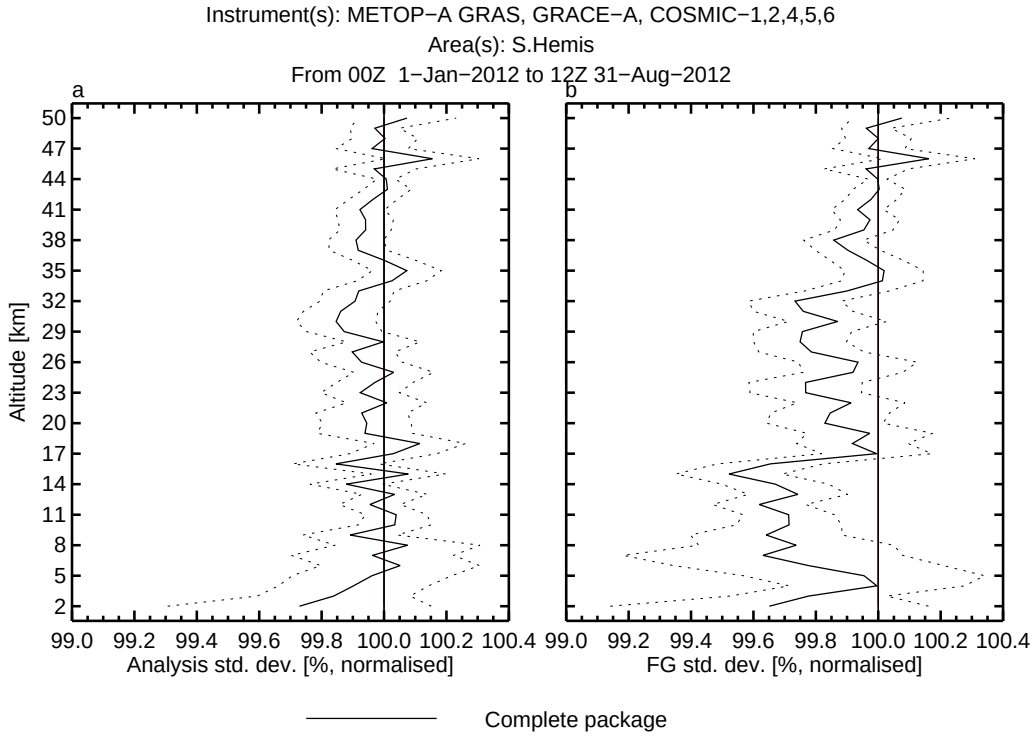

Figure 18: As Fig. 17 but for GPSRO observations in the southern hemisphere. The 95% confidence range is represented by light dotted lines.

This also gives a hint that it may be the unbalanced winds that are improved in the analysis. However, the size of the changes is small and further investigation would be necessary to confirm these ideas.

The main information content of the observations is water vapour, cloud and precipitation, so improvements in fits to mid- and upper-tropospheric humidity sounding channels are expected; changes are around 0.5% to 1% and are statistically at analysis and FG. Fits to the humidity sounding channels of HIRS are shown in Fig. 19, channels 11 and 12); similar results are seen with MHS, IASI and AIRS (not shown).

4 Conclusion

Cycle 40r1 will include a package of changes to the all-sky assimilation of microwave imagers that is based on improvements to the radiative transfer model in frozen precipitation which eliminate the largest remaining bias in the all-sky FG departures. This has allowed the extension of all-sky assimilation into deep-convective areas at higher frequencies (e.g. 37 GHz and 92 GHz channels) and to the 183 GHz humidity sounding channels of SSMIS. This all-sky upgrade brings 1% improvements in humidity forecasts and 0.5% improvements in wind forecasts. These are seen in many parts of the troposphere both in the FG departures and in the first 3 to 4 days of forecast scores, where they are statistically significant. The wind improvements are largest in the winter storm tracks where 4D-Var tracing of water vapour, cloud and precipitation is the likely mechanism, though further work would be needed to be certain. There is even a suggestion that longer-range forecast scores (e.g. days 5 to 8) are improved in the SH through knock-on improvements in the stratospheric polar vortex.

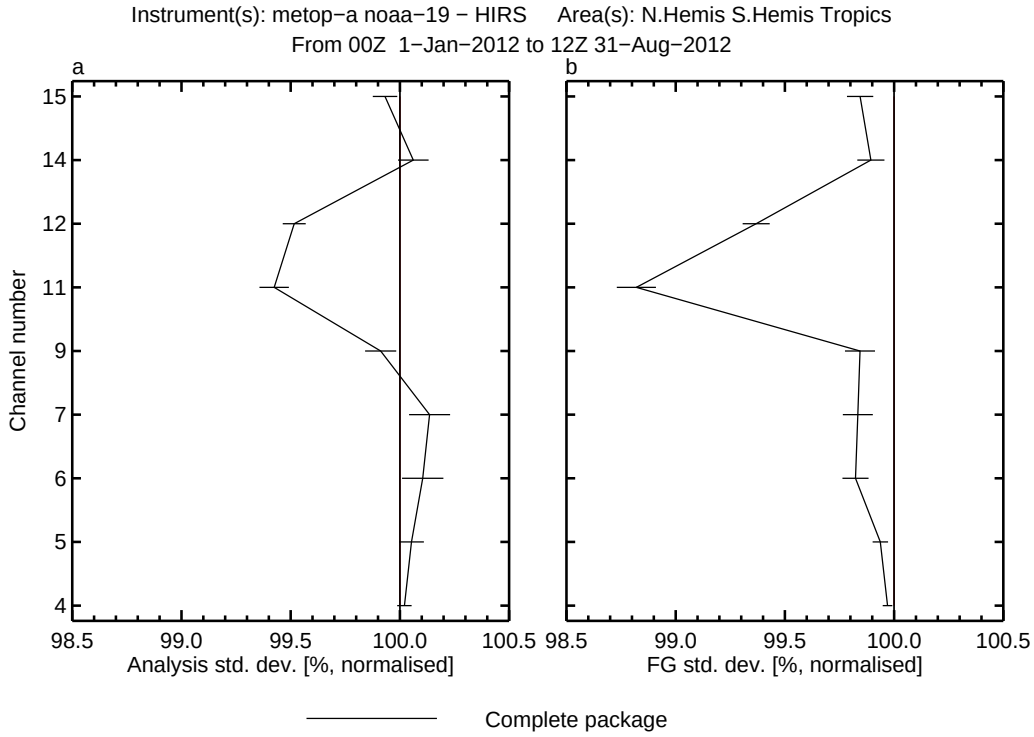

Figure 19: As Fig. 17 but for global HIRS observations.

Testing the components of the all-sky package separately has shown that all-sky assimilation of SSMIS 183 GHz channels is responsible for much of the improvement in winds the storm track regions, as well as improvements in humidity through the troposphere. This type of channel has previously only been assimilated in clear-skies, but in that configuration there is little benefit to dynamical forecasts. All-sky assimilation brings much greater observational coverage at high latitudes and gives the potential for 4D-Var tracing to work on cloud and precipitation as well as humidity. Further, the clear-sky assimilation of these channels is affected by biases due to ineffective cloud-detection. Given the success of the SSMIS all-sky 183 GHz assimilation, it is worth trying the assimilation of the MHS 183 GHz channels in the all-sky path rather than in the clear-sky path. Also, humidity sounding channels in the IR have similarities in their radiative transfer so they too may bring benefits if assimilated in an all-sky approach.

Acknowledgements

This work has depended on the contribution of many people but particularly on that of Bill Bell, Fabrizio Baordo, Stephen English, Peter Bauer, Enza Di Tomaso, Niels Bormann, Reima Eresmaa, Jean-Noël Thépaut and Anne Fouilloux.

References

Allen, D. R., K. W. Hoppel, G. E. Nedoluha, D. D. Kuhl, N. L. Baker, L. Xu, and T. E. Rosmond (2013). Limitations of wind extraction from 4D-Var assimilation of ozone. *Atmos. Chem. Phys. 13,*

3501–3515.

Andersson, E., E. Hólm, P. Bauer, A. Beljaars, G. A. Kelly, A. P. McNally, A. J. Simmons, J.-N. Thépaut, and A. Tompkins (2007). Analysis and forecast impact of the main humidity observing systems. *Quart. J. Roy. Meteorol. Soc. 133*, 1473–1485.

Andersson, E., J. Pailleux, J. N. Thépaut, J. R. Eyre, A. P. McNally, G. A. Kelly, and P. Courtier (1994). Use of cloud-cleared radiances in three/four-dimensional variational data assimilation. *Quart. J. Roy. Meteorol. Soc. 120*, 627–653.

Baordo, F., A. J. Geer, and S. English (2012). SSMI/S radiances over land in the all-sky framework: one year report. *EUMETSAT/ECMWF Fellowship Programme Research Report No. 27, available from http://www.ecmwf.int*.

Bauer, P., A. J. Geer, P. Lopez, and D. Salmond (2010). Direct 4D-Var assimilation of all-sky radiances: Part I. Implementation. *Quart. J. Roy. Meteorol. Soc. 136*, 1868–1885.

Bauer, P., E. Moreau, F. Chevallier, and U. O'Keeffe (2006). Multiple-scattering microwave radiative transfer for data assimilation applications. *Quart. J. Roy. Meteorol. Soc. 132*, 1259–1281.

Bell, W., B. Candy, N. Atkinson, F. Hilton, N. Baker, N. Bormann, G. Kelly, M. Kazumori, W. Campbell, and S. Swadley (2008). The assimilation of SSMIS radiances in numerical weather prediction models. *IEEE Trans. Geosci. Remote Sensing 46*, 884–900.

Buehler, S. A. and V. O. John (2005). A simple method to relate microwave radiances to upper tropospheric humidity. *Journal of Geophysical Research: Atmospheres 110*.

Draine, B. T. and P. J. Flatau (1994). Discrete-dipole approximation for scattering calculations. *J. Opt. Soc. Am. A 11*, 1491–1499.

Eyre, J. R. (1991). A fast radiative transfer model for satellite sounding systems. *ECMWF Tech. Memo., 176, available from http://www.ecmwf.int*.

Field, P. R., A. J. Heymsfield, and A. Bansemer (2007). Snow size distribution parameterization for midlatitude and tropical ice clouds. *J. Atmos. Sci. 64*, 4346 – 4365.

Geer, A. J. and F. Baordo (2013). Improved scattering radiative transfer for frozen hydrometeors at microwave frequencies. *to be submitted to Atmos. Meas. Tech.*.

Geer, A. J. and P. Bauer (2010). Enhanced use of all-sky microwave observations sensitive to water vapour, cloud and precipitation. *Published simultaneously as ECMWF Technical Memoranda 620 and ECMWF/EUMETSAT fellowship reports 20.*

Geer, A. J. and P. Bauer (2011). Observation errors in all-sky data assimilation. *Quart. J. Roy. Meteorol. Soc. 137*, 2024–2037.

Geer, A. J., P. Bauer, and N. Bormann (2010a). Solar biases in microwave imager observations assimilated at ECMWF. *IEEE Trans. Geosci. Remote Sens. 48*, 2660 – 2669.

Geer, A. J., P. Bauer, and S. J. English (2012). Assimilating AMSU-A temperature sounding channels in the presence of cloud and precipitation. *Published simultaneously as ECMWF Technical Memoranda 670 and ECMWF/EUMETSAT fellowship reports 24*.

Geer, A. J., P. Bauer, and P. Lopez (2010b). Direct 4D-Var assimilation of all-sky radiances: Part II. Assessment. *Quart. J. Roy. Meteorol. Soc. 136*, 1886–1905.

Geer, A. J., P. Bauer, and C. W. O'Dell (2009). A revised cloud overlap scheme for fast microwave radiative transfer. *J. App. Meteor. Clim. 48*, 2257–2270.

Gopalan, K., L. Jones, S. Biswas, S. Bilanow, T. Wilheit, and T. Kasparis (2009). A time-varying radiometric bias correction for the TRMM microwave imager. *IEEE Trans. Geosci. Remote Sensing 47*, 3722–3730.

Hong, G., G. Heygster, J. Miao, and K. Kunzi (2005). Detection of tropical deep convective clouds from AMSU-B water vapor channels measurements. *J. Geophys. Res. 110*, D05205.

Joseph, J., W. J. Wiscombe, and J. A. Weinman (1976). The delta-Eddington approximation for radiative flux transfer. *J. Atmos. Sci. 33*, 2452–2459.

Kulie, M. S., R. Bennartz, T. J. Greenwald, Y. Chen, and F. Weng (2010). Uncertainties in microwave properties of frozen precipitation: implications for remote sensing and data assimilation. *J. Atmos. Sci. 67*, 3471–3487.

Kummerow, C., W. Barnes, T. Kozu, J. Shiue, and J. Simpson (1998). The Tropical Rainfall Measuring Mission (TRMM) sensor package. *J. Atmos. Ocean. Tech. 15*, 809–817.

Kunkee, D., G. Poe, D. Boucher, S. Swadley, Y. Hong, J. Wessel, and E. Uliana (2008). Design and evaluation of the first Special Sensor Microwave Imager/Sounder. *IEEE Trans. Geosci. Remote Sensing 46*, 863–883.

Liu, G. (2008). A database of microwave single-scattering properties for nonspherical ice particles. *Bull. Am. Met. Soc. 111*, 1563–1570.

Lopez, P. and E. Moreau (2005). A convection scheme for data assimilation: Description and initial tests. *Quart. J. Roy. Meteorol. Soc. 131*, 409–436.

Petty, G. W. and W. Huang (2010). Microwave backscatter and extinction by soft ice spheres and complex snow aggregates. *J. Atmos. Sci. 67*, 769–787.

Peubey, C. and A. P. McNally (2009). Characterization of the impact of geostationary clear-sky radiances on wind analyses in a 4D-Var context. *Quart. J. Roy. Meteorol. Soc. 135*, 1863 – 1876.

Peuch, A., J. N. Thepaut, and J. Pailleux (2000). Dynamical impact of total-ozone observations in a four-dimensional variational assimilation. *Quart. J. Roy. Meteorol. Soc. 126*, 1641 – 1659.

Purcell, E. D. and C. R. Pennypacker (1973). Scattering and absorption of light by nonspherical dielectric grains. *Astrophys. J. 186*, 705 – 714.

Riishøjgaard, L. P. (1996). On four-dimensional variational assimilation of ozone data in weather-prediction models. *Quart. J. Roy. Meteorol. Soc. 122*, 1545–1571.

Saunders, R., J. Hocking, P. Rayer, M. Matricardi, A. Geer, N. Bormann, P. Brunel, F. Karbou, and F. Aires (2012). RTTOV-10 science and validation report. NWPSAF-MO-TV-023 v1.11, EUMETSAT NWP-SAF.

Tompkins, A. M. and M. Janisková (2004). A cloud scheme for data assimilation: Description and initial tests. *Quart. J. Roy. Meteorol. Soc. 130*, 2495–2517.